American Mineralogist, Volume 81, pages 995–1002, 1996

A new hyper-calcic amphibole with Ca at the A site: Fluor-cannilloite from Pargas, Finland

FRANK C. HAWTHORNE,[1,*] ROBERTA OBERTI,[1] LUCIANO UNGARETTI,[1] AND JOEL D. GRICE[2]

[1]CNR Centro di Studio per la Cristallochimica e la Cristallografia, via Abbiategrasso 209, I-27100 Pavia, Italy
[2]Research Division, Canadian Museum of Nature, P.O. Box 3443, Station "D", Ottawa, Ontario K1P 6P4, Canada

ABSTRACT

Electron microprobe analysis of amphiboles from Pargas, Finland, shows up to 2.42 Ca apfu (atoms per formula unit), far in excess of the usual maximum value of 2.00 Ca apfu observed in amphiboles. The most Ca-rich composition is $(K_{0.12}Na_{0.35}Ca_{0.52})(Ca_{1.92}Mn^{2+}_{0.05}Fe^{2+}_{0.03})(Mg_{3.73}Fe^{2+}_{0.43}Ti_{0.02}Al_{0.82})(Si_{5.63}Al_{2.37})O_{22}[(OH)_{0.46}F_{1.54}]$. Fluor-cannilloite, ideally $CaCa_2(Mg_4Al)(Si_5Al_3)O_{22}F_2$, is a new amphibole species in which Ca is dominant at the A site. Fluor-cannilloite occurs as isolated anhedral grains and small granular aggregates in a marble together with calcite, muscovite, anorthite, aluminous diopside, pyrope, and fluorite. It is grayish green with a grayish white streak, brittle, $H = 6$, $D_{meas} = 3.05$ g/cm^3, and shows perfect {110} cleavage. In plane-polarized light, it is pale greenish gray to almost colorless, rather cloudy and mottled in appearance, and is not pleochroic. Fluor-cannilloite is biaxial positive, $\alpha = 1.611(2)$, $\beta = 1.616(2)$, $\gamma = 1.633(2)$, $2V = 49(2)°$, dispersion weak $r > v$. It is monoclinic, space group $C2/m$, $a = 9.826(4)$, $b = 17.906(9)$, $c = 5.301(3)$ Å, $\beta = 105.41(4)°$, $V = 899.2$ Å^3, $Z = 2$. The ten strongest X-ray diffraction lines in the powder pattern [d in Å(I)(hkl)] are 8.936(4)(020), 8.355(3)(110), 3.366(4)(131), 3.107(7)(310), 2.686(10)(151), 2.578(10)(061), 2.328(4)($\bar{3}$51), 2.165(6)(171), 2.036(5)(202), 1.435(9)($\bar{4}$.10.1).

The structures of fluor-cannilloite and another Ca-rich amphibole from Madagascar were refined to R indices of ~1.5% using reflection intensities collected with Mo$K\alpha$ X radiation. Site populations were assigned from the refined site-scattering values, considerations of mean bond lengths, and the unit formulas calculated from the electron microprobe analyses. Both the electron microprobe data and the site-scattering refinements show significant Ca (up to 0.52 apfu) together with Na and K at the A site. Both A2 and Am sites are occupied, with the A2 site having the higher electron density. Local bond-valence considerations indicate that Ca is equally partitioned between the A2 and Am sites, whereas K occupies Am and Na occupies A2.

INTRODUCTION

In all discussions of amphibole compositions, Ca is assigned to the B group (Ernst 1968; Leake 1968; Deer et al. 1963; Ungaretti 1980; Hawthorne 1981, 1983), i.e., Ca is considered to occupy only the M4 site in the $C2/m$ amphibole structure. Compositional data suggesting that Ca occurs at any other site (i.e., at the A site or the M1, M2, or M3 sites) are considered to be seriously in error (Robinson et al. 1981).

During a systematic examination of amphibole crystal chemistry, we discovered amphiboles with anomalously high contents of Ca, rather ironically from Pargas, Finland. The most Ca-rich crystals had Ca exceeding 0.5 occupancy of the A site and hence constitute a new amphibole species. It has been named fluor-cannilloite, partly for the composition but primarily for Elio Cannillo (b. 1938) of Pavia, Italy, for his contribution to our understanding of the crystal chemistry of rock-forming minerals, particularly pyroxenes and amphiboles. The species and name have been approved by the International Mineralogical Association Commission on New Minerals and Mineral Names; holotype material is deposited at the Canadian Museum of Nature, Ottawa.

As well as being of general interest with regard to amphibole crystal chemistry, this particular amphibole obviously will affect our evaluation of the quality of amphibole analyses in the future. Consequently, we characterized this amphibole, both chemically and structurally, to confirm the initial findings and to elucidate the role of "excess" Ca in the structure. Later we learned that pargasite with significant excess Ca was reported by Moine et al. (1985) in urano-thorianite–bearing pyroxenite from southeastern Madagascar. In the present study we also examine pargasite (sample BMS) from this locality, con-

* Present address: Department of Geological Sciences, University of Manitoba, Winnipeg, Manitoba R3T 2N2, Canada.

0003–004X/96/0708–0995$05.00

TABLE 1. Electron microprobe analysis (wt%) and unit formulas (apfu) of fluor-cannilloite and Ca-rich pargasite (BMS)

	C1	C2	C3	BMS
SiO_2	39.52	38.78	38.75	43.04
Al_2O_3	18.05	18.74	18.58	13.76
TiO_2	0.24	0.18	0.13	0.44
FeO	3.23	3.19	3.54	—
Fe_2O_3	—	—	—	1.92
MnO	0.37	0.41	0.48	0.03
MgO	17.87	17.54	17.02	20.36
CaO	15.78	15.73	15.45	14.16
Na_2O	1.46	1.22	1.25	1.62
K_2O	0.23	0.66	0.80	2.21
F	3.20	3.66	2.92	3.43
H_2O*	(0.56)	(0.48)	(0.67)	(0.47)
O = F	−1.35	−1.54	−1.23	−1.44
Total	99.16	98.79	98.36	100.00
Si	5.701	5.607	5.656	6.121
Al	2.299	2.393	2.344	1.879
Σ	8.000	8.000	8.000	8.000
Al	0.770	0.801	0.853	0.427
Ti	0.026	0.020	0.014	0.047
Fe^{2+}	0.390	0.386	0.432	—
Fe^{3+}	—	—	—	0.205
Mn^{2+}	0.045	0.050	0.059	0.004
Mg	3.844	3.782	3.704	4.317
ΣC	5.075	5.039	5.063	5.000
Mn,Fe^{2+}	0.075	0.039	0.063	—
Ca	2.439	2.437	2.416	2.158
Σ	2.514	2.476	2.479	2.158
Ca	0.514	0.476	0.479	0.158
Na	0.408	0.342	0.354	0.447
K	0.042	0.122	0.149	0.401
ΣA	0.965	0.940	0.982	1.006
F	1.46	1.67	1.35	1.54
OH	(0.54)	(0.33)	(0.65)	(0.46)
ΣO(3)	2.00	2.00	2.00	2.00

* Calculated assuming OH + F = 2 apfu.

firming that it contains Ca at the A site and showing that Ca at the A site in amphibole is not a local oddity.

SAMPLE PROVENANCE AND PARAGENESIS

The sample in which fluor-cannilloite occurs is from Pargas, Finland, and is in the Mineralogy Museum of the Dipartimento di Scienze della Terra, Università di Pavia, sample 9680; it was collected in the nineteenth century. The hand specimen, an equidimensional sample about 2 cm in diameter, is a marble consisting primarily of calcite together with cannilloite, muscovite, anorthite, an aluminous diopside, pyrope, and fluorite.

Pargasite BMS from southeastern Madagascar (Tranomaro region) occurs in urano-thorianite–bearing pyroxenite for which the proposed conditions of regional metamorphism are T = 700–750 °C, $P \leq 5$ kbar, and log f_{F_2} is in the range −33 to −31. More details about the mineralogy and petrology of these rocks can be found in Moine et al. (1985).

PHYSICAL AND OPTICAL PROPERTIES

Fluor-cannilloite is gray-green and semitranslucent with a vitreous luster; it has a grayish white streak and shows no fluorescence under long-wave or short-wave ultraviolet light. It occurs as isolated anhedral grains and small granular aggregates up to 0.15 × 0.15 × 0.20 mm in diameter. Fluor-cannilloite has a Mohs hardness of ~6 and is brittle. It has the characteristic perfect {110} cleavage of monoclinic amphiboles, intersecting at ~56°. The density, measured by flotation, is 3.05(3) g/cm³ in comparison with a calculated value of 3.18 g/cm³.

A spindle stage was used to orient three crystals for refractive index measurements and determination of $2V$ by extinction curves. The optical orientation was determined by transferring crystals from the spindle stage to a precession camera and determining the relative axial relationships by X-ray diffraction. In transmitted light, fluor-cannilloite is pale grayish green to almost colorless with a cloudy and mottled appearance; it is not pleochroic and shows no discernable differential absorption. It is biaxial positive with indices of refraction α = 1.611(2), β = 1.616(2), γ = 1.633(2), measured with gel-filtered Na light (λ = 589.9 nm). The $2V$ value is 49(2)° and dispersion is weak, $r > v$.

CHEMICAL COMPOSITION

Fluor-cannilloite and BMS pargasite were analyzed primarily by electron microprobe using a CAMECA SX-50 operating in wavelength-dispersive mode with the following conditions: excitation voltage 15 kV, specimen current 20 nA, peak count time 20 s, background count time 10 s, using the standards and data reduction procedure described by Hawthorne et al. (1992). The principal zoning observed is K ⇌ Na. Analyses of individual grains (Table 1) are the mean of 10–20 analytical points and are representative of the average composition of each crystal. The Fe^{3+}/Fe^{2+} ratios were derived from stereochemical considerations related to the crystal-structure refinement results (namely, the agreement between observed and calculated octahedral mean bond distances). There was insufficient material for an H_2O determination. Unit formulas were calculated on the basis of 24(O,OH,F), assuming OH + F = 2 apfu (atoms per formula unit).

X-RAY CRYSTALLOGRAPHY

X-ray precession photographs taken with Zr-filtered Mo$K\alpha$ X radiation are compatible with Laue symmetry $2/m$, and the conditions for reflections to be present, $h + k = 2n$, show that the lattice is C centered. The possible space groups are $C2/m$, $C2$, and Cm, and crystal-structure refinement confirmed the space group $C2/m$. The powder diffraction pattern was recorded using Cu$K\alpha$ X-radiation, a Gandolfi camera, and a few very small crystals, and cell dimensions were refined using the program Celref (Appleman and Evans 1973); the indexed powder pattern and refined cell dimensions are given in Table 2.

Three crystals, C1–C3, from the same hand specimen from Pargas were used for crystallographic measurements; one (BMS) is from the Madagascar sample. Unit-cell dimensions (Table 3) and intensity data were measured in the θ range 2–30° on a Philips PW 1100 four-circle diffractometer using graphite-monochromated

TABLE 2. X-ray powder diffraction data for fluor-cannilloite

I/I_o	d_{meas} (Å)	d_{calc} (Å)	*hkl*
4	8.936	8.944	020
3	8.355	8.371	110
1	5.041	5.046	$\bar{1}30$
1	3.874	3.871	$\bar{1}31$
4	3.365	3.364	131
4	3.247	3.251	240
10	3.107	3.109	310
1	2.788	2.790	330
10	2.686	2.688	151
10	2.578	2.575	061
1	2.460	2.457	022
4	2.328	2.329	$\bar{3}51$
3	2.283	2.284	$\bar{1}71$
1	2.283	2.284	$\bar{3}12$
6	2.165	2.165	171
5	2.036	2.037	202
3	2.004	2.003	351
1	1.987	1.986	222
2	1.870	1.870	$\bar{4}61$
1	1.764	1.764	312
1	1.608	1.607	$\bar{6}21$
4	1.579	1.579	600
4	1.547	1.547	402
3	1.504	1.505	$\bar{3}92$
9	1.435	1.435	$\bar{4}101$
1	1.398	1.398	$\bar{7}11$
4	1.354	1.354	313
3	1.332	1.332	$\bar{6}23$
3	1.332	1.331	1112
1	1.304	1.304	1131
3	1.286	1.286	$\bar{2}122$

Note: $a = 9.814(2)$, $b = 17.887(3)$, $c = 5.295(1)$ Å, $\beta = 105.17(2)°$.

Mo$K\alpha$ X radiation according to the experimental procedure of Oberti et al. 1993. The crystals used in the collection of the X-ray intensity data were subsequently analyzed with a fully automated Cameca SX-50 electron microprobe according to the procedure of Hawthorne et al. (1992).

Crystal structures were refined to R indices of ~1.5% using the procedure described by Oberti et al. (1993). No weights and no constraints were used during the refinement; a reflection was considered as observed if $F_{obs} > 5\sigma_{F_{obs}}$. Atomic coordinates and equivalent isotropic displacement factors are given in Table 4, structure factors and anisotropic displacement factors are listed in Table 5, and selected interatomic distances and refined site-

TABLE 3. Unit-cell dimensions and crystal-structure refinement information for fluor-cannilloite and Ca-rich pargasite

	C1	C2	C3	BMS
a (Å)	9.816(10)	9.826(4)	9.836(5)	9.889(2)
b (Å)	17.899(21)	17.906(9)	17.921(9)	17.978(3)
c (Å)	5.297(6)	5.301(3)	5.306(3)	5.298(2)
β (°)	105.35(8)	105.41(4)	105.40(4)	105.41(2)
V (Å^3)	897.5	899.2	901.7	908.1
SEQ*	645	644	358	662
No. F_{all}	1364	1362	1365	1380
No. F_{obs}	904	1048	1027	1125
R_{sym} (%)	1.9	1.1	1.8	1.4
R_{obs} (%)	1.7	1.3	1.5	1.7
R_{all} (%)	3.4	2.3	2.5	2.4

* SEQ = sequence number in Pavia amphibole database.

TABLE 4. Atomic fractional coordinates and equivalent isotropic displacement parameters (Å^2)

		C1	C2	C3	BMS
O1	x	0.1057	0.1053	0.1053	0.1064
	y	0.0875	0.0878	0.0880	0.0872
	z	0.2156	0.2153	0.2154	0.2179
	B_{eq}	0.81	0.78	0.81	0.74
O2	x	0.1197	0.1194	0.1194	0.1193
	y	0.1730	0.1732	0.1733	0.1726
	z	0.7367	0.7371	0.7373	0.7323
	B_{eq}	0.70	0.67	0.70	0.70
O3	x	0.1076	0.1072	0.1075	0.1056
	y	0	0	0	0
	z	0.7149	0.7149	0.7152	0.7143
	B_{eq}	0.98	0.95	0.93	0.79
O4	x	0.3674	0.3675	0.3675	0.3660
	y	0.2517	0.2518	0.2519	0.2508
	z	0.7895	0.7899	0.7896	0.7916
	B_{eq}	0.92	0.89	0.89	0.90
O5	x	0.3532	0.3531	0.3531	0.3503
	y	0.1413	0.1415	0.1414	0.1394
	z	0.1149	0.1153	0.1153	0.1121
	B_{eq}	1.01	0.94	0.93	1.0
O6	x	0.3457	0.3457	0.3454	0.3453
	y	0.1167	0.1167	0.1168	0.1175
	z	0.6142	0.6156	0.6156	0.6110
	B_{eq}	1.08	1.04	1.04	1.0
O7	x	0.3451	0.3448	0.3444	0.3411
	y	0	0	0	0
	z	0.2755	0.2766	0.2773	0.2871
	B_{eq}	1.21	1.23	1.26	1.24
T1	x	0.2819	0.2815	0.2814	0.2798
	y	0.0855	0.0857	0.0857	0.0855
	z	0.3044	0.3049	0.3050	0.3051
	B_{eq}	0.50	0.48	0.48	0.49
T2	x	0.2919	0.2918	0.2919	0.2903
	y	0.1737	0.1738	0.1738	0.1733
	z	0.8156	0.8163	0.8165	0.8141
	B_{eq}	0.50	0.46	0.46	0.52
M1	x	0	0	0	0
	y	0.0894	0.0895	0.0896	0.0892
	z	½	½	½	½
	B_{eq}	0.58	0.56	0.55	0.53
M2	x	0	0	0	0
	y	0.1753	0.1753	0.1754	0.1756
	z	0	0	0	0
	B_{eq}	0.56	0.51	0.51	0.52
M3	x	0	0	0	0
	y	0	0	0	0
	z	0	0	0	0
	B_{eq}	0.58	0.55	0.55	0.56
M4	x	0	0	0	0
	y	0.2795	0.2797	0.2800	0.2796
	z	½	½	½	½
	B_{eq}	0.71	0.69	0.61	0.74
M4′	x	0	0	0	—
	y	0.2657	0.2655	0.2692	—
	z	½	½	½	—
	B_{eq}	2.66	1.14	1.16	—
A	x	0	0	0	0
	y	½	½	½	½
	z	0	0	0	0
	B_{eq}	4.90	5.39	6.29	0.91
Am	x	0.0515	0.0576	0.0521	0.0321
	y	½	½	½	½
	z	0.1089	0.1212	0.1107	0.0681
	B_{eq}	3.76	1.40	2.97	2.99
A2	x	0	0	0	0
	y	0.4675	0.4680	0.4675	0.4729
	z	0	0	0	0
	B_{eq}	1.98	2.72	1.71	2.77
H	x	—	—	—	0.1688
	y	—	—	—	0
	z	—	—	—	0.6402
	B_{eq}	—	—	—	7.9

Note: Standard deviations are ≤1 on the last decimal place.

TABLE 6. Selected interatomic distances (Å) and angles (°) in fluor-cannilloite and Ca-rich pargasite

	C1	C2	C3	BMS		C1	C2	C3	BMS
T1-O1	1.668	1.670	1.670	1.654	T2-O2	1.630	1.634	1.636	1.630
T1-O5	1.693	1.696	1.698	1.688	T2-O4	1.603	1.606	1.609	1.600
T1-O6	1.689	1.693	1.694	1.679	T2-O5	1.645	1.644	1.645	1.649
T1-O7	1.674	1.677	1.678	1.664	T2-O6	1.660	1.660	1.660	1.665
⟨T1-O⟩	1.681	1.684	1.685	1.671	⟨T2-O⟩	1.635	1.636	1.638	1.636
M1-O1 × 2	2.043	2.045	2.046	2.044	M3-O1 × 4	2.051	2.054	2.058	2.062
M1-O2 × 2	2.101	2.102	2.105	2.093	M3-O3 × 2	2.059	2.059	2.061	2.054
M1-O3 × 2	2.082	2.083	2.088	2.079	⟨M3-O⟩	2.054	2.056	2.059	2.060
⟨M1-O⟩	2.075	2.076	2.079	2.072					
					M4-O2 × 2	2.409	2.411	2.416	2.415
M2-O1 × 2	2.054	2.049	2.051	2.078	M4-O4 × 2	2.327	2.332	2.334	2.351
M2-O2 × 2	2.048	2.047	2.047	2.073	M4-O5 × 2	2.587	2.583	2.583	2.631
M2-O4 × 2	1.970	1.967	1.967	1.987	M4-O6 × 2	2.569	2.571	2.570	2.567
⟨M2-O⟩	2.024	2.021	2.022	2.046	⟨M4-O⟩	2.473	2.474	2.476	2.491
A-O5 × 4	3.051	3.057	3.059	3.048	Am-O5 × 2	3.197	3.228	3.207	3.129
A-O6 × 4	3.032	3.029	3.034	3.062	Am-O5 × 2	3.043	3.057	3.054	3.022
A-O7 × 2	2.370	2.379	2.388	2.460	Am-O6 × 2	2.597	2.552	2.593	2.780
					Am-O7	2.414	2.442	2.432	2.466
A2-O5 × 2	2.589	2.601	2.597	2.662	Am-O7	3.148	3.080	3.134	3.332
A2-O6 × 2	2.665	2.666	2.666	2.749	Am-O7	2.504	2.538	2.527	2.523
A2-O7 × 2	2.440	2.448	2.458	2.508					
					T1-O5-T2	132.5	132.5	132.5	133.7
A2-O3	3.790	3.796	3.799	3.821	T1-O6-T2	136.7	136.5	136.6	136.2
Am-O3	3.226	3.175	3.228	3.459	T1-O7-T1	132.3	132.4	132.6	134.9
O5-O6-O5	160.9	160.8	160.8	163.0					
O5-O7-O5	141.8	141.7	141.5	138.3					

Note: Standard deviations are 1 in the last digit for both distances and angles.

scattering values in epfu (electrons per formula unit) are given in Tables 6 and 7, respectively.[1]

SITE POPULATIONS

The unit formulas calculated from the EMP data can be used to calculate the effective scattering [at $(\sin\theta)/\lambda = 0$] from the A-, B-, and C-group cations [where A, B, and C refer to $^{[6-12]}$(A, Am, A2), $2^{[8]}$(M4, M4′), $^{[6]}$(2M1, 2M2, M3), respectively]. These values may also be derived by summing the refined site-scattering values of the various sites within each group from structure refinement (SREF). Values are compared in Table 7. The overall scattering values from the two sets of results are in close agreement; for the individual group sites, the scattering at B and C from SREF are higher, whereas those at A are lower. In this particular case, the A-site scattering from SREF may be low because of difficulties in modeling the A-site electron density with the usual three-site model (see the next paragraph for further details). The presence of the split M4′ site with a more suitable [6 + 2] coordination (Oberti et al. 1993) in the case of C1–C3 confirms the (Mn^{2+},Fe^{2+}) content of the B group indicated by the electron microprobe analyses. Complete site populations are reported in Table 7.

A site

This is the site of major interest here because the unit formulas indicate that the A site is approximately half-occupied by Ca in crystals C1–C3. The refined site scattering from the A site confirms this assignment, being reasonably compatible with the site populations assigned from the unit formulas. There are three sites within the A cavity: A2/m (A), Am, and A2, which are named after their point symmetry. The assignment of Ca to one of these sites is difficult because of the simultaneous presence of three chemical species, namely Na, K, and Ca (for a detailed discussion on Na and K partitioning within the A cavity, see Hawthorne et al. 1996). The electron density at the A site (Figs. 1a and 1b) is elongated both along the twofold axis (Fig. 1a) and in the mirror plane (Fig. 1b), indicating significant occupancy of both the A2 and the Am sites. A section through the A site on $(\bar{2}01)$ contains both the A2 and Am sites (Fig. 1c) and best shows the distribution of electron density in the A cavity. There are two prominent maxima at the A2 sites on the twofold axis, indicating that the maximum electron density is at this site. Very close contouring of the electron density (Fig. 1d) also shows two subsidiary maxima at the Am sites on the mirror plane and a minimum in the electron density at the central A2/m site. These maps thus show the electron-density distribution A2 > Am. In accord with this, the site-scattering values of the A2 and Am sites were refined; however, this model left a small amount of residual electron density at the central A2/m site. This site cannot be occupied by K, Na, or Ca because the resulting interatomic distances are too long to satisfy the bond-valence requirements of the central cation. Such residual electron density presumably results from difficulties in accounting for positional disorder at the A2 and Am sites owing to variation in occupancy of neighboring

[1] A copy of Table 5 may be ordered as Document AM-96-620 from the Business Office, Mineralogical Society of America, 1015 Eighteenth Street NW, Suite 601, Washington, DC 20036. Please remit $5.00 in advance for the microfiche.

TABLE 7. Refined site-scattering (epfu) from SREF and EMP,* and the complete site-group populations obtained from SREF + EMP results

	N**	C1	C2	C3	BMS
			SREF		
M1	2	25.81	25.99	26.08	24.16
M2	2	28.25	28.20	28.37	27.24
M3	1	12.98	13.10	13.19	12.22
ΣM1,2,3		67.04	67.29	67.64	63.62
M4,4′	2	40.70	40.65	40.29	40.00
A	1	14.69	15.35	15.79	15.29
Total		122.79	123.29	123.72	118.91
			EMP		
M1,2,3		66.06	66.54	66.97	63.82
M4		40.41	40.21	40.32	40.00
A		15.57	15.60	16.30	15.70
Total		122.04	122.35	123.59	119.52
			A		
Na		0.41	0.34	0.35	0.44
K		0.04	0.12	0.15	0.40
Ca		0.51	0.48	0.48	0.16
			M4		
Ca		1.93	1.92	1.94	2.00
Mn^{2+}		0.04	0.05	0.06	—
Fe^{2+}		0.03	0.03	—	—
			M1		
Mg		1.88	1.86	1.84	2.00
Fe^{2+}		0.12	0.14	0.16	0.00
			M2		
Mg		0.98	0.94	0.90	1.42
Al		0.78	0.82	0.84	0.36
Ti		0.02	0.02	0.02	0.04
Fe^{2+}		0.22	0.22	0.24	0.00
Fe^{3+}		0.00	0.00	0.00	0.18
			M3		
Mg		0.93	0.92	0.92	0.90
Fe^{2+}		0.07	0.08	0.08	0.02
Al		0.00	0.00	0.00	0.08
			T1		
Si		1.71	1.63	1.66	2.14
Al		2.29	2.37	2.34	1.86
			T2		
Si		4.00	4.00	4.00	4.00
			O3		
OH		0.54	0.46	0.65	0.46
F		1.46	1.54	1.35	1.54

* Standard deviations are in the range 2–12 in the last digit.
** N = number of sites in the structural formula.

sites (e.g., F vs. OH at O3, Hawthorne et al. 1996). In the refinement procedure, the occupancy of the central A2/m site was refined together with the parameters of the A2 and Am sites to produce the observed amount of scattering at the A site. This procedure produces good agreement with the total scattering at the A site. However, because of problems with resolution owing to the close approach of the three sites (Hawthorne et al. 1996), the individual occupancies of the three sites are not given. The true stereochemistry within the A cavity is better derived from the difference-Fourier map (Fig. 1), which indicates A2 > Am, together with the observation that the central A2/m site cannot be occupied.

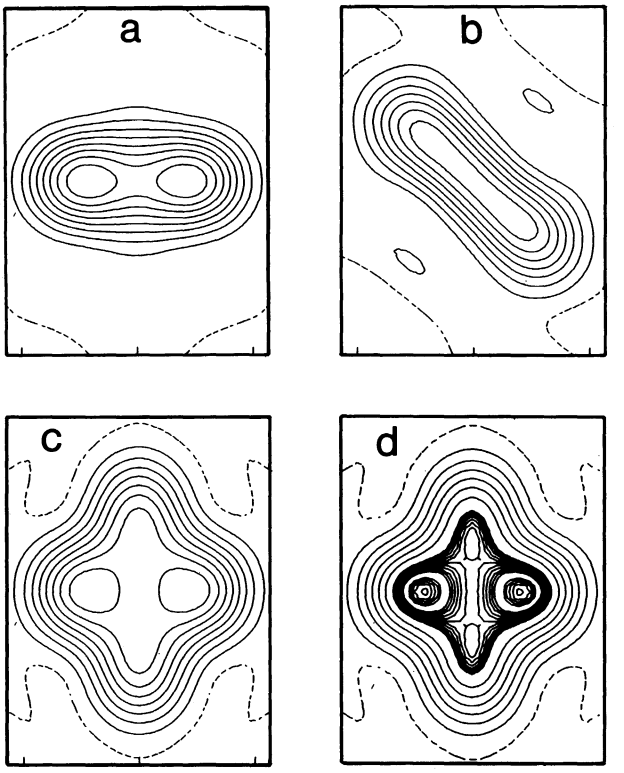

FIGURE 1. Difference-Fourier sections for fluor-cannilloite calculated through the central A2/m site with the A cation removed from the structural model (the contour interval is 1 e/Å³): (**a**) (100) section at $x = 0$; (**b**) (010) section at $y = 1/2$; (**c**) section through the electron-density maxima on the twofold axis and in the mirror plane, parallel to ($\bar{2}01$); (**d**) the ($\bar{2}01$) section with 0.1 e/Å³ contouring above 6 e/Å³.

T, B, and C sites

Tetrahedrally coordinated Al significantly exceeds 2.0 apfu for the crystals from Pargas C1–C3, and the ⟨T1-O⟩ and ⟨T2-O⟩ distances indicate that $^{[4]}$Al is very strongly ordered at T1. These Al contents at T1 are significantly higher than the usual limit of 2.0 apfu, and for all crystals examined SREF data indicate that $^{[4]}$Al at T2 is below the limit of detectability of the method used (Table 7).

Both SREF and EMP results for C1–C3 show the M4 cavity to be occupied by Ca plus small amounts of C-group cations of higher scattering power than Ca, the latter being ordered at the M4′ site; of the available C-group cations, Mn^{2+} generally shows the strongest site preference for M4 and was so assigned, together with minor amounts of Fe^{2+}. For crystal BMS, the absence of Mn^{2+} and Fe^{2+} in the unit formula (Table 1) is compatible with only Ca at M4 (Table 7) and the lack of a split M4′ site in this crystal.

Octahedral site populations (Table 7) were obtained for all the crystals using EMP and SREF data (in particular, observed mean bond distances and site scatterings), with the constraint of electroneutrality of the unit formula,

TABLE 8. Simple bond-valence model for local coupling of ^{T1}Al-O7-^{T1}Al linkages with Ca at the A site

	^{A}Na	^{T1}Al	^{T1}Si	Σ
O7	0.25	0.75	1.00	2.00
	^{A}Ca	^{T1}Al	^{T1}Al	Σ
O7	0.50	0.75	0.75	2.00

according to the procedure of Ungaretti et al. (1983). Note that Fe^{3+} is calculated to be 0 apfu for C1–C3, whereas it is calculated to be nearly total Fe for BMS.

A CRYSTAL-CHEMICAL MODEL FOR THE Ca → (Na, K) SUBSTITUTION AT THE A SITE

The presence of ~0.5 Ca apfu at the A site and an Al content at the T1 site in excess of 2.0 apfu can be related by the substitution ^{A}Ca + $^{[4]}$Al → ^{A}Na + Si. Ca orders at the off-centered A2 and Am positions to satisfy its bond-valence requirements. In this way, further bond valence may also be contributed to the O5, O6, and O7 anions, all of which are linked to tetrahedral cations. Indeed, the Am-O6 and A2-O5 bonds in fluor-cannilloite are among the shortest bonds from the A cation to O5 and O6 observed in monoclinic amphiboles. In normal amphiboles, the Al content of the T1 site rarely exceeds 2.0 apfu because this would force Al-O7-Al linkages and the bond-valence requirements of the bridging O7 atom could not be satisfied (Oberti et al. 1995). Consequently, $^{[4]}$Al in excess of 2 apfu is incorporated at the T2 site; although there are well-documented examples of this (Hawthorne and Grundy 1977; Oberti et al. 1995), it is unfavorable from a bond-valence viewpoint. The O4 anion is bonded to the T2, M2, and M4 cations, and the occurrence of Al at T2 leads to local problems in satisfying the incident bond-valence requirements of O4. In fluor-cannilloite, the presence of Ca at the A site overcomes the problem of Al-O-Al linkages through O7, and the resulting occurrence of >2 Al apfu at T1 relieves the bond-valence problems at O4 by allowing all $^{[4]}$Al to occur at the T1 site.

Table 8 shows a simple bond-valence model for the O7 site, approximating the T1-O7 bond valence by 1.0 and 0.75 vu for T1 = Si and T1 = Al, respectively. When the linkage through O7 is Si-O7-Al, the bond-valence requirements of O7 are satisfied by the two T1 cations and Na at the A site. When the linkage through O7 is Al-O7-Al, the bond-valence requirements are satisfied by the two T1 cations and Ca at the A site. When A = Na, the bond-valence requirements of the O7 anion do not allow Al-O7-Al linkages; when A = Ca, the Ca contribution to O7 is sufficient to allow Al-O7-Al linkages. Thus, Loewenstein's rule and this violation of it are simple consequences of the valence-sum rule (Brown 1981).

Figure 2 shows the coordination of the A2 and Am sites in fluor-cannilloite. Both the A2 and Am cations bond to two O7 atoms at about the same distance (~2.47 Å). However, A2 bonds to two O7 anions diagonally across the A cavity (Fig. 2a), whereas the Am atom bonds to two O7 anions on one side of the A cavity (Fig. 2b). There are two possible relations between Al-O7-Al linkages in the chain above the A cavity relative to the chain below the A cavity: The linkages can lie diagonally across the A cavity (Fig. 2c), or they can both lie to one side of the A cavity (Fig. 2d). When the Al-O7-Al linkages lie diagonally across the A cavity, the bond-valence requirements of both O7 anions can be satisfied by Ca at the A2 position (Fig. 2c). When the Al-O7-Al linkages lie to one side of the A cavity, the bond-valence requirements of both O7 anions can be satisfied by Ca at the Am position (Fig. 2d). Because both arrangements of Al-O7-Al linkages shown in Figure 2 are equally probable, Ca should be partitioned equally between A2 and Am. If this model is correct, we should be able to calculate the scattering at the A2 and Am sites from the unit formulas (Table 1), as K occupies the Am site and ^{A}Na occupies the A2 site. For the crystals C1–C3, this procedure gives site-scattering values at A2 and Am of 9.0 and 6.6 epfu, respectively, in good agreement with the Fourier maps of Figure 1 and the refined scattering at the A2 and Am sites.

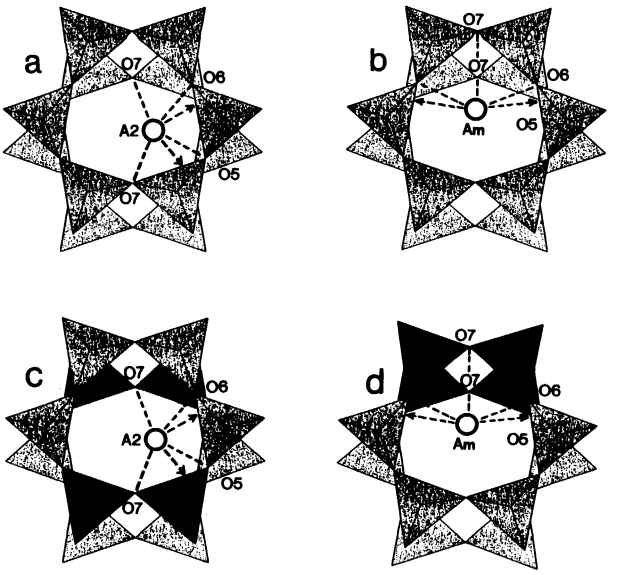

FIGURE 2. Coordination around the A2 and Am sites in fluor-cannilloite: (**a**) A2 site projected onto (100); (**b**) Am site projected onto (100). In **c** and **d**, tetrahedra occupied by Al are shaded black, and tetrahedra occupied by Si are dot shaded.

This crystal-chemical model confirms the importance of the ^{A}Ca + $^{[4]}$Al → ^{A}Na + Si substitution, which gives the ideal end-member $CaCa_2(Mg_4Al)Si_5Al_3O_{22}(OH)_2$ of Figure 2a. The substitution ^{A}Ca + $^{[6]}$Mg → ^{A}Na + $^{[6]}$Al, which produces the end member $CaCa_2Mg_5(Si_6Al_2)O_{22}F_2$, when evaluated from the crystal-chemical viewpoint, does

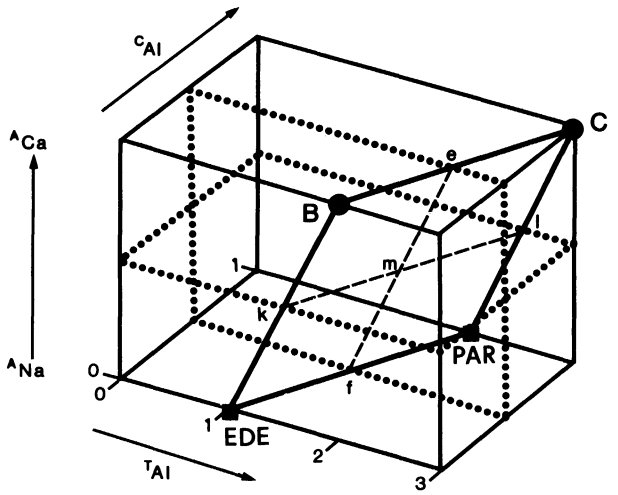

FIGURE 3. ACT compositional diagram for A-site–full calcic fluor-amphiboles. The A axis shows the Na ⇌ Ca substitution, the C axis shows the $M^{2+} \rightleftharpoons M^{3+}$ substitution (written as ^{C}Al), and the T axis shows the Si ⇌ Al substitution (written as ^{T}Al). Compositions marked are as follows: EDE = $NaCa_2Mg_5(Si_7Al)O_{22}F_2$, PAR = $NaCa_2(Mg_4Al)(Si_6Al_2)O_{22}F_2$, B = $CaCa_2Mg_5(Si_6Al_2)O_{22}F_2$, C = $CaCa_2(Mg_4Al)(Si_5Al_3)O_{22}F_2$.

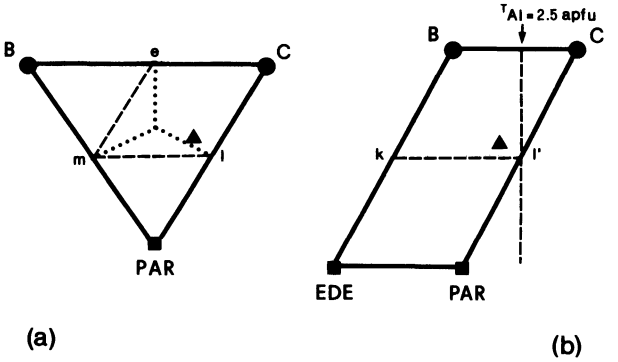

FIGURE 4. The PAR-B-C plane from Figure 3. (a) Orthogonal view; the intersection of the planes ^{A}Ca = 0.5 and ^{C}Al = 0.5 apfu with this quadrilateral are shown by broken lines. (b) Projected onto the AT plane; the intersection of the planes ^{A}Ca = 0.5 and ^{T}Al = 5.5 apfu with the projected quadrilateral are shown by broken lines. The fluor-cannilloite composition C1 (Table 1) is shown by the solid triangle.

not allow an efficient mechanism for achieving local charge balance at the O5, O6, and O7 anions.

CHEMICAL CONSIDERATIONS

Heterovalent substitutions in amphiboles can occur at each of the four groups of sites: A, B, C, and T. For the amphiboles of Table 1, the B group is filled with divalent cations, predominantly Ca, and hence their compositional relationship to other amphiboles can be expressed in ACT space (Fig. 3) for A-site–filled compositions. In Figure 3, the base of the parallelepiped represents calcic amphiboles with the A site filled with Na, and the top surface represents compositions with the A site filled with Ca. Two compositions are possible on this top surface, B = $CaCa_2Mg_5(Si_6Al_2)O_{22}F_2$ and C = $CaCa_2(Mg_4Al)(Si_5Al_3)O_{22}F_2$, and calcic amphibole compositions (with B = Ca_2) are confined to the edenite-pargasite-C-B plane. Figure 4a shows the pargasite-B-C plane with the composition of type fluor-cannilloite marked. Putting aside, for the moment, the fact that fluor-cannilloite is an amphibole, such a ternary system is normally divided into three species as shown by the dotted lines (Nickel 1992). From this, it is quite clear that fluor-cannilloite would fall into the compositional field of C rather than B. Figure 4b shows the same plane projected onto the AT plane, as is conventionally done for the purposes of amphibole nomenclature. Now the type composition for fluor-cannilloite lies closest to composition B in projection. This provides us with something of a conundrum, as the standard criteria for amphibole nomenclature would assign B as the ideal end-member composition of fluor-cannilloite, whereas both Figure 4a and the crystal-chemical mechanism indicate the ideal end-member to be C. This situation arises because the A-, B-, and T-group cations are used in the standard amphibole classification scheme, rather than the A-, B-, and C-group cations. In our view, it is crystal chemically more reasonable to approximate $(Si_{5.62}Al_{2.38})$ by (Si_5Al_3) than it is to approximate $(Mg^*_{4.16}Al^*_{0.84})$ by (Mg^*_5) with Mg* = Mg + Fe^{2+} and Al* = Al + Ti. Thus, we prefer to give the ideal end-member composition of fluor-cannilloite as $CaCa_2(Mg_4Al)(Si_5Al_3)O_{22}F_2$.

Leake (1968) listed seven analyses of amphiboles from Pargas, Finland. One is from a hornblendite and thus not relevant to the current discussion; the other analyses are of amphiboles in marbles, and these are listed in Table 9. First, there seems to be significant compositional variation in amphiboles from this locality, with edenite (210, 223), fluor-pargasitic hornblende (378), ferroan pargasitic hornblende (479), and fluor-pargasite (492, 1011). Second, a particular feature of the more aluminous compositions is their high Ca contents (mean of 1.98 Ca apfu), although these are significantly below the values (mean of 2.43 Ca apfu) found in the present study. Third, three of the four Al-rich compositions show significant occupancy of the B group by smaller divalent (Fe^{2+}, Mn^{2+}, Mg) cations. This occurrence of Fe^{2+}, Mn^{2+}, and Mg at the B group is a common feature of calcic amphiboles, although the values for the amphiboles of Table 9 are much higher than usual (this could be the result of underestimation of the H_2O content by use of the Penfield method), as are the total cation contents. Decreasing the Fe^{2+}, Mn^{2+}, and Mg contents to the values obtained in this study still results in Ca occupancy of the A site; the one exception is 1011. Thus, the previous analyses of fluor-pargasite and related amphiboles from Pargas, Finland, do suggest the presence of Ca at the A site, although not in the large quantities observed here.

TABLE 9. Chemical analyses and unit formulas of amphiboles from marbles at Pargas, Finland (from Leake 1968)

	210	223	378	479	492	1011
SiO_2	48.38	48.10	43.90	42.05	41.90	42.09
Al_2O_3	10.83	11.05	12.52	12.60	14.90	13.60
TiO_2	0.05	0.10	0.70	0.91	0.46	0.68
Fe_2O_3	0.76	0.67	0.38	1.68	1.90	2.06
FeO	1.50	1.65	5.95	11.51	3.50	5.45
MnO	0.04	—	—	—	0.06	0.07
MgO	20.76	20.60	18.91	13.48	18.54	16.16
CaO	12.24	12.50	12.69	11.85	13.11	13.40
Na_2O	2.69	2.54	1.34	1.97	2.33	2.16
K_2O	1.38	1.24	1.30	1.90	1.46	1.43
F	1.82	1.90	2.29	1.82	3.06	2.65
H_2O	0.91	0.71	0.51	0.41	0.35	0.82
O = F	−0.76	−0.80	−0.96	−0.76	−1.29	−1.12
Total	100.68	100.37	99.63	99.41	100.30	99.45
Si	6.76	6.76	6.35	6.33	6.04	6.15
Al	1.24	1.24	1.65	1.67	1.96	1.85
ΣT	8.00	8.00	8.00	8.00	8.00	8.00
Al	0.54	0.58	0.49	0.57	0.58	0.49
Ti	0.00	0.01	0.08	0.10	0.05	0.07
Fe^{3+}	0.08	0.07	0.04	0.18	0.21	0.23
Fe^{2+}	0.18	0.18	0.72	1.45	0.43*	0.68*
Mg	4.33	4.32	4.10	3.03	3.99	3.52
ΣC	5.13	5.16	5.43	5.33	5.26	4.99
Δ	0.13	0.16	0.43	0.33	0.26	—
Ca	1.82	1.88	1.97	1.90	2.03	2.04
Na	0.05	—	—	—	—	—
ΣB	2.00	2.04	2.40	2.23	2.29	2.04
Ca	—	0.04	0.40	0.23	0.29	0.04
Na	0.48	0.69	0.38	0.58	0.65	0.61
K	0.03	0.24	0.24	0.36	0.27	0.27
ΣA	0.51	0.97	1.02	1.17	1.21	0.92
F	0.84	0.84	1.04	0.87	1.40	1.22
OH	0.80	0.67	0.50	0.41	0.33	0.80
O^{2-}	0.36	0.49	0.46	0.72	0.27	—

* Includes 0.01 Mn.

Do other amphibole analyses in the literature show similar features [apart from those by Moine et al. (1985)]? In Leake (1968), there are 31 analyses in which Ca exceeds 2.10 apfu; 21 of these have additional "unsatisfactory" features, specifically total cation contents significantly in excess of 16 apfu, T-cation sums much less than 8 apfu, or C-cation sums much less than 5 apfu. The remainder have Ca contents in the range 2.10–2.21 apfu; some of these may have excess Ca at the A site, but usually the parageneses show no Ca-excess phase, and so it is difficult to be convinced by these analyses. Thus, there seems to be little good evidence as to the previous detection of significant Ca at the A site in amphibole. However, the Pargas paragenesis hardly seems geologically uncommon, and examination of marbles from other localities should surely give amphiboles with compositions similar to those recorded in Table 9.

ACKNOWLEDGMENTS

Bernard Moine is gratefully acknowledged for kindly providing the pargasite from Madagascar. F.C.H. was supported by a Killam Fellowship, CNR-NATO, and an operating grant from the Natural Sciences and Engineering Research Council of Canada.

REFERENCES CITED

Appleman, D.E., and Evans, H.T., Jr. (1973) Job 9214: Indexing and least-squares refinement of powder diffraction data. U.S. National Technical Information Service, Document PB 216 188.

Brown, I.D. (1981) The bond-valence method: An empirical approach to chemical structure and bonding. In M. O'Keeffe and A. Navrotsky, Eds., Structure and bonding in crystals II, p. 1–30. Academic, New York.

Deer, W.A., Howie, R.A., and Zussman, J. (1963) Rock-forming minerals, vol. 2: Chain silicates, 379 p. Longman and Green, London.

Ernst, W.G. (1968) Amphiboles: Crystal chemistry, phase relations and occurrence, 125 p. Springer-Verlag, New York.

Hawthorne, F.C. (1981) Crystal chemistry of the amphiboles. In Mineralogical Society of America Reviews in Mineralogy, 9A, 1–102.

——— (1983) The crystal chemistry of the amphiboles. Canadian Mineralogist, 21, 173–480.

Hawthorne, F.C., and Grundy, H.D. (1977) The crystal chemistry of the amphiboles: III. Refinement of the crystal structure of a sub-silicic hastingsite. Mineralogical Magazine, 41, 43–50.

Hawthorne, F.C., Oberti, R., Ungaretti, L., and Grice, J.D. (1992) Leakeite, $NaNa_2(Mg_2Fe^{3+}_3Li)Si_8O_{22}(OH)_2$, a new alkali amphibole from the Kajlidongri manganese mine, Jhabua district, Madhya Pradesh, India. American Mineralogist, 77, 1112–1115.

Hawthorne, F.C., Oberti, R., and Sardone, N. (1996) Sodium at the A site in clinoamphiboles: The effects of composition on ordering patterns. Canadian Mineralogist, in press.

Leake, B.E. (1968) A catalog of analyzed calciferous and subcalciferous amphiboles together with their nomenclature and associated minerals. Geological Society of America, Special Paper 98.

Moine, B., Rakotondratsima, C., and Cuney, M. (1985) Les pyroxénites à urano-thorianite du Sud-East de Madagascar: Conditions physico-chimiques de la métasomatose. Bulletin de Minéralogie, 108, 325–340.

Nickel, E.H. (1992) Solid solutions in mineral nomenclature. Canadian Mineralogist, 30, 231–234.

Oberti, R., Hawthorne, F.C., Ungaretti, L., and Cannillo, E. (1993) The behaviour of Mn in amphiboles: Mn in richterite. European Journal of Mineralogy, 5, 43–51.

Oberti, R., Ungaretti, L., Cannillo, E., Hawthorne, F.C., and Memmi, I. (1995) Temperature-dependent Al order-disorder in the tetrahedral double-chain of *C2/m* amphiboles. European Journal of Mineralogy, 7, 1049–1063.

Robinson, P., Speer, F.S., Schumacher, J.C., Laird, J., Klein, C., Evans, B.W., and Doolan, B.L. (1981) Phase relations of metamorphic amphiboles: Natural occurrence and theory. In Mineralogical Society of America Reviews in Mineralogy, 9B, 1–227.

Ungaretti, L. (1980) Recent developments in X-ray single-crystal diffractometry applied to the crystal-chemical study of amphiboles. Godisniak Jugoslavenskog Centra za Kristalografiju, 15, 29–65.

Ungaretti, L., Lombardo, B., Domeneghetti, C., and Rossi, G. (1983) Crystal-chemical evolution of amphiboles from eclogitised rocks of the Sesia Lanzo Zone, Italian Western Alps. Bulletin de Minéralogie, 106, 645–672.

MANUSCRIPT RECEIVED JULY 14, 1995
MANUSCRIPT ACCEPTED MARCH 25, 1996